J Neurophysiol 116: 1840–1847, 2016.
First published July 27, 2016; doi:10.1152/jn.00513.2016.

Magnetoencephalography-based identification of functional connectivity network disruption following mild traumatic brain injury

Ahmad Alhourani,[1] Thomas A. Wozny,[1] Deepa Krishnaswamy,[2] Sudhir Pathak,[2] Shawn A. Walls,[5] Avniel S. Ghuman,[1,2,3,4] Donald N. Krieger,[1] David O. Okonkwo,[1] R. Mark Richardson,[1,2,4] and Ajay Niranjan[1]

[1]*Department of Neurological Surgery, University of Pittsburgh School of Medicine, Pittsburgh, Pennsylvania;* [2]*Department of Neurobiology, University of Pittsburgh School of Medicine, Pittsburgh, Pennsylvania;* [3]*Department of Psychiatry, University of Pittsburgh School of Medicine, Pittsburgh, Pennsylvania;* [4]*Center for the Neural Basis of Cognition and University of Pittsburgh Brain Institute, University of Pittsburgh, Pittsburgh, Pennsylvania; and* [5]*University of Pittsburgh Medical Center Brain Mapping Center, Pittsburgh, Pennsylvania*

Submitted 24 June 2016; accepted in final form 25 July 2016

Alhourani A, Wozny TA, Krishnaswamy D, Pathak S, Walls SA, Ghuman AS, Krieger DN, Okonkwo DO, Richardson RM, Niranjan A. Magnetoencephalography-based identification of functional connectivity network disruption following mild traumatic brain injury. *J Neurophysiol* 116: 1840–1847, 2016. First published July 27, 2016; doi:10.1152/jn.00513.2016.—Mild traumatic brain injury (mTBI) leads to long-term cognitive sequelae in a significant portion of patients. Disruption of normal neural communication across functional brain networks may explain the deficits in memory and attention observed after mTBI. In this study, we used magnetoencephalography (MEG) to examine functional connectivity during a resting state in a group of mTBI subjects ($n = 9$) compared with age-matched control subjects ($n = 15$). We adopted a data-driven, exploratory analysis in source space using phase locking value across different frequency bands. We observed a significant reduction in functional connectivity in band-specific networks in mTBI compared with control subjects. These networks spanned multiple cortical regions involved in the default mode network (DMN). The DMN is thought to subserve memory and attention during periods when an individual is not engaged in a specific task, and its disruption may lead to cognitive deficits after mTBI. We further applied graph theoretical analysis on the functional connectivity matrices. Our data suggest reduced local efficiency in different brain regions in mTBI patients. In conclusion, MEG can be a potential tool to investigate and detect network alterations in patients with mTBI. The value of MEG to reveal potential neurophysiological biomarkers for mTBI patients warrants further exploration.

traumatic brain injury; magnetoencephalography; functional connectivity; resting-state analysis; graph theory; default mode network; concussion; phase locking value

NEW & NOTEWORTHY

We demonstrate that 2 min of resting MEG recordings carry adequate information to detect network changes following mTBI and to localize the cortical areas responsible for these network changes. These changes can be reliably detected months after the initial injury (median of 8 mo) despite normal anatomical imaging.

TRAUMATIC BRAIN INJURY (TBI) represents an immense and growing source of morbidity and mortality, accounting for ~2.5 million emergency department visits, hospitalizations, and deaths annually in the United States (Centers for Disease Control and Prevention 2014). Notably, mild TBI (mTBI) accounts for 75% of all TBI cases (Centers for Disease Control and Prevention 2003), and a considerable portion of these patients develop persistent cognitive deficits (van der Naalt et al. 1999; Vanderploeg et al. 2005). Strikingly little is known about the pathophysiology underlying these cognitive symptoms, since conventional structural brain imaging techniques have not been successful in identifying biomarkers of mTBI (Van Boven et al. 2009).

Persistent postconcussion symptoms include a cluster of somatic, affective, and cognitive symptoms (Cicerone and Kalmar 1995). The cognitive symptoms include memory problems, difficulty in concentration, mental fogginess, fatigue, and mental slowing. This constellation of symptoms represents diverse higher cognitive functions distributed across different functional cortical networks. The heterogeneity of mTBI mechanisms suggests that common network disruptions could explain this relatively reproducible cluster of symptoms, rather than localized injury to any particular brain region (Sharp et al. 2014). Higher-order cognitive functions involve efficient information processing across spatially disparate neuronal populations. The theory of communication through coherence (Fries 2015) proposes that this long-range information transfer is facilitated by synchronization in the phase of local neuronal oscillations between functionally connected nodes. Functional connectivity within brain networks, therefore, can be identified through measures of interregional synchrony.

Functional imaging modalities are powerful tools that can complement standard structural imaging, such as CT and MRI, by measuring interregional synchrony in brain function. Magnetoencephalography (MEG), specifically, is capable of quickly and noninvasively measuring pan-cortical brain activity with a higher degree of combined spatial and temporal resolution than is possible with functional MRI (fMRI) or scalp EEG. Several MEG studies provide evidence for network disruption after TBI generally (Tarapore et al. 2013) and mTBI specifically (Castellanos et al. 2011; Dimitriadis et al. 2015; Dunkley et al. 2015).

In this study, we quantified the local and global functional connectivity specific to multiple frequency bands in patients with mTBI and age-matched control subjects. We used a

Address for reprint requests and other correspondence: A. Niranjan, Dept. of Neurosurgery, Univ. of Pittsburgh, Suite B-400, UPMC Presbyterian, 200 Lothrop St., Pittsburgh, PA 15213 (e-mail: niranjana@upmc.edu).

Table 1. *mTBI group subject characteristics*

Subject	Sex	Age, yr	Mechanism of Injury
T1	Female	30	MVA
T2	Male	15	Sports related
T3	Male	29	MVA
T4	Female	14	Sports related
T5	Male	52	Sports related
T6	Female	62	MVA
T7	Male	29	Blast and blunt
T8	Male	28	Blunt trauma
T9	Female	29	Fall

mTBI patient characteristics in terms of age, sex, and mechanism of injury. MVA, motor vehicle accident.

data-driven approach to identify robust network changes at the source dipole level. We aimed to describe the topology of the network disruption at the source level after mTBI and whether the affected areas would include parts of the default mode network (DMN). Finally, graph theory measures were applied to provide a descriptive measure of alterations in network topology.

METHODS

Subject population. Data were collected retrospectively with the following inclusion criteria: a documented history of head injury, Glasgow coma scale of 14 or 15 at presentation, age between 14 and 75 yr, and persistent postconcussion symptoms. Exclusion criteria included history of neurological or psychiatric illness, including substance abuse, and contraindications to MRI, including implanted devices, such as pacemakers, as well as pregnancy. Nine subjects (4 women, 5 men) were recruited in the mTBI group with a mean age of 33.1 ± 5.2 yr (SE). Only one subject had a blast-related injury (Table 1). Scans were performed at the University of Pittsburgh Medical Center at a median of 8 mo after injury (range 3–96 mo). Healthy control subjects consisted of 15 subjects with a mean age of 24.9 (range 22–36) yr. The two groups were not statistically different in terms of age ($P > 0.05$). Informed consent was obtained prior to MEG scans, in accordance with a protocol approved by the Institutional Review Board of the University of Pittsburgh.

Data acquisition. Data analysis was performed with resting-state data (Fig. 1). Resting, eyes-open recordings were obtained with an Elekta-Neuromag VectorView 306-channel system with a sampling rate of 1,000 Hz (0.03 Hz high-pass online filter, 330-Hz antialiasing low-pass online filter). Recording time varied between 3 and 5 min for each subject. A 2- to 5-min empty-room recording, with the same acquisition parameters and with no subject present in the magnetically shielded room, was obtained on the same day. Same-day empty-room recordings were not available for the mTBI group, so the most temporally proximal empty-room sessions were used for each patient.

Data preprocessing. All recordings were visually inspected for time segments and channels that were obviously contaminated with artifact, both of which were marked and excluded from further analysis. The data were then notch filtered at 60 Hz and harmonics with an ideal filter implemented in MATLAB. Signals were then low-pass filtered at 240 Hz and high-pass filtered at 1 Hz with

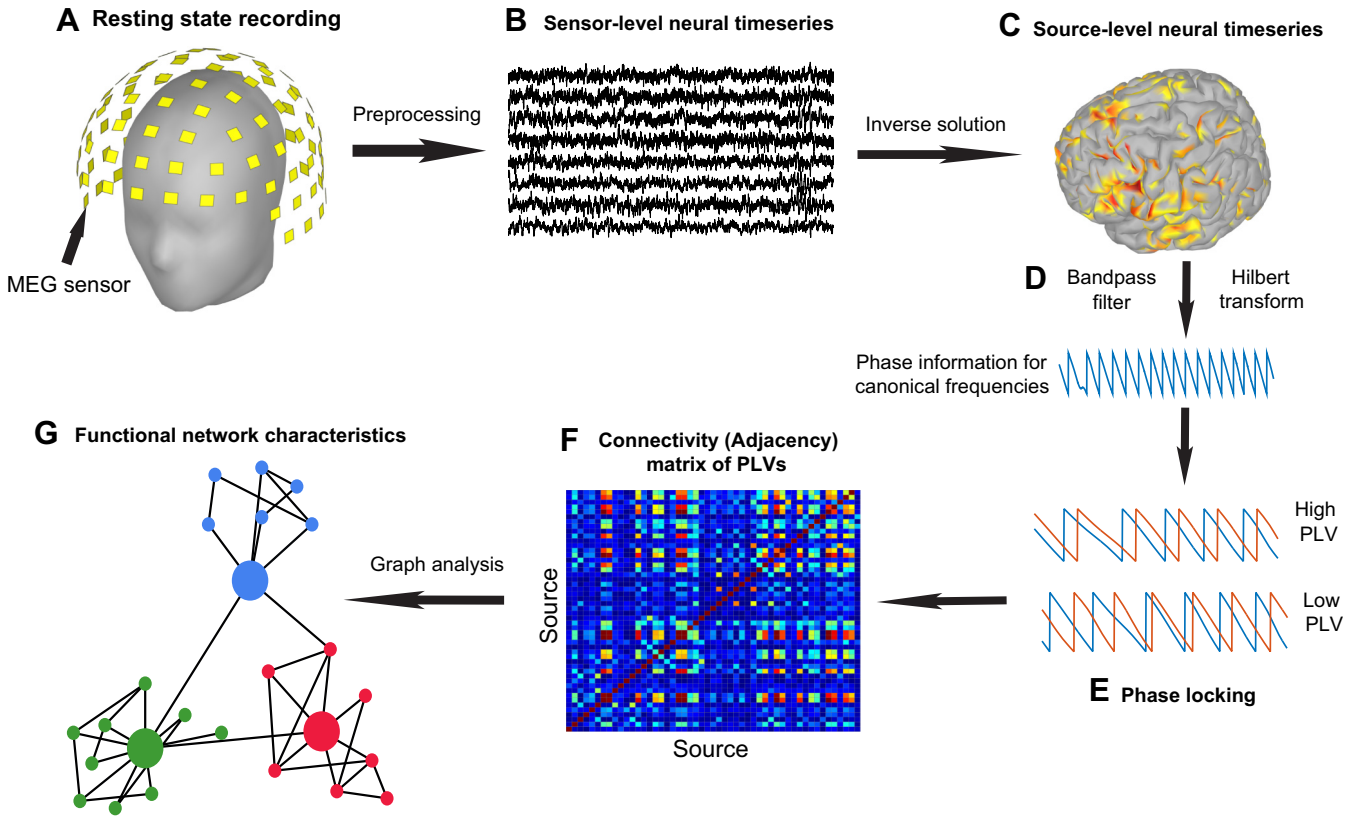

Fig. 1. Analysis stream for resting-state functional connectivity using 5,000 dipoles across the cortical surface. *A*: resting-state MEG data were collected with a 306-Elekta machine. *B*: resting-state recordings were preprocessed to obtain 2 min of artifact-free neural time series at the sensor level. *C*: cortical activity was estimated with minimum norm estimate inverse solution. *D*: the source dipoles were band-pass filtered into canonical frequency band, and a Hilbert transform was applied to derive estimates of instantaneous phase. *E*: phase locking value (PLV) for each pairwise combination of source dipoles was calculated to construct a connectivity matrix representing the PLVs between all the source dipoles (*F*). Each connectivity matrix was submitted to graph analysis to describe the functional organization of the network (*G*).

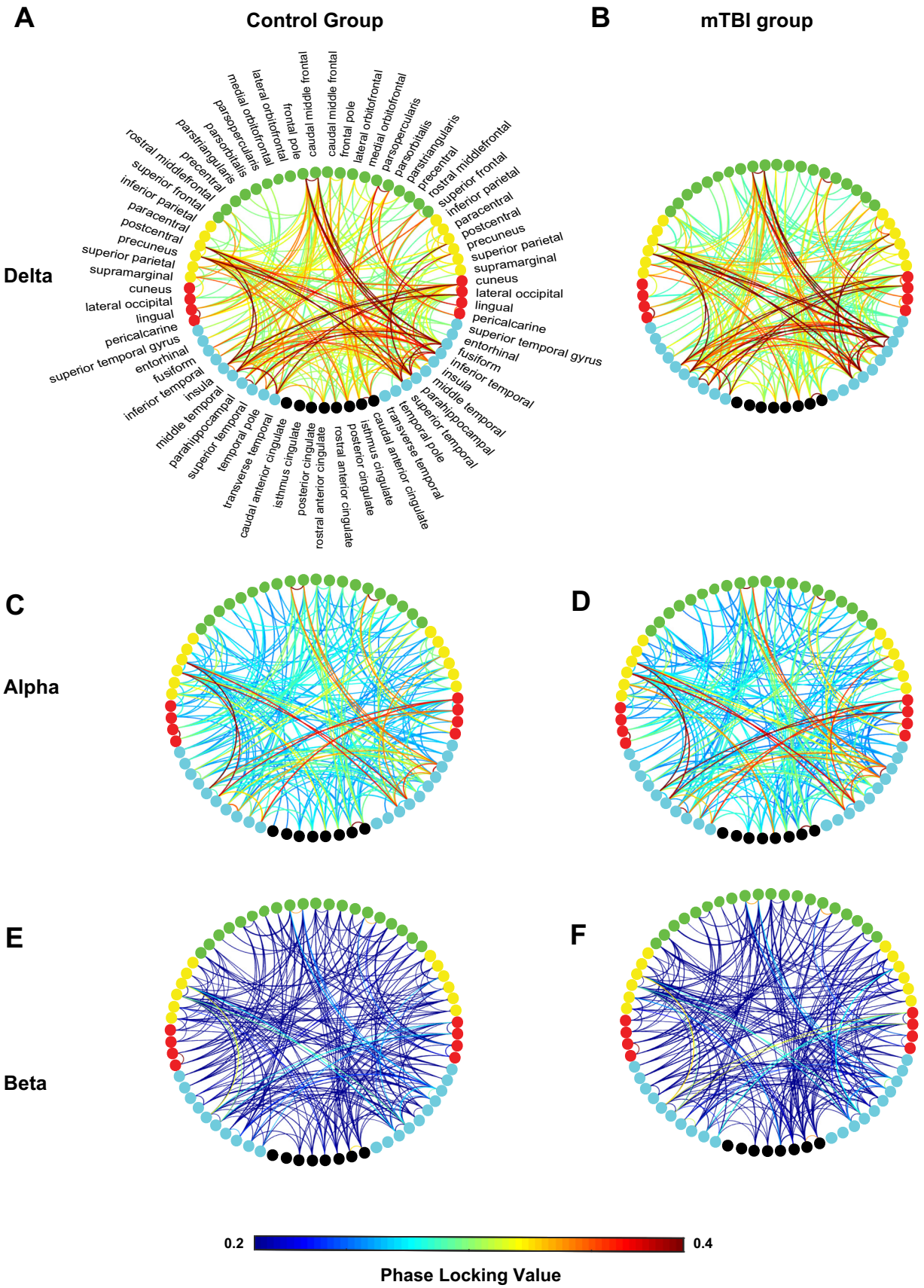

zero-phase finite impulse response (FIR) filters prior to downsampling to 500 Hz. Heartbeat and eyeblink-related artifacts were isolated and removed with an Infomax ICA-based procedure (Liu et al. 2010). Structural MRI images were obtained for each subject with a 3-T whole body scanner (Siemens). A T1-weighted brain volume was used to generate a cortical surface model with the FreeSurfer software package. The individual surfaces were used to coregister between the MEG fiducial markers and the MRI structural images. Some aspects of the data preprocessing and MEG source imaging were performed with Brainstorm (Tadel et al. 2011). The resultant cortical surface mesh was downsampled to 5,000 vertices in total.

Forward modeling of magnetic field activity was performed with the overlapping-sphere method implemented in Brainstorm (Huang et al. 1999) with a loose dipolar orientation constraint value of 0.4 for the calculation of the weighted minimum norm estimate W:

$$W = A^T\left(AA^T + \lambda C\right)^{-1}$$

Here A represents the gain matrix as calculated from the forward solution and C is the spatial covariance of the noise of the recordings (Baillet et al. 2001). Typically, in task-related scans, the noise covariance can be estimated from the times the subject is not performing the task. However, in the case of resting-state scans, such an estimate would diminish the spontaneous covariance in the data. To this end, the noise covariance matrix was constructed from each subject's respective empty-room recording (Ghuman et al. 2011). The subject recordings were registered to a common template with the FreeSurfer spherical registration method (Fischl et al. 1999). The MNI ICBM152 template was used as the surface template after downsampling the high-resolution surface to roughly 5,000 triangle vertices. Anatomical regions of interest (ROIs) were defined automatically with FreeSurfer (Destrieux et al. 2010).

Functional connectivity analysis. Functional connectivity was estimated with phase locking value (PLV) (Lachaux et al. 1999). Briefly, dipolar source activity was band-pass filtered with an FIR filter as implemented in EEGLAB (Delorme and Makeig 2004) into the canonical frequency bands of delta (1–4 Hz), theta (4–8 Hz), alpha (8–12 Hz), and beta (12–30 Hz). For the beta band, five narrow nonoverlapping bands from 12 to 28 Hz in 4-Hz steps were used. The instantaneous phase was then estimated with the Hilbert transform. The PLV for frequency band f between sources i and j was defined as

$$\mathrm{PLV}(i,j) = \left| \frac{1}{N} \sum_{n=1}^{N} e^{i(\varphi i - \varphi j)} \right|$$

where N is the number of time points in the time series and φ represents the phase of the band-passed data at frequency band f for sources i and j. The values for PLV are bounded between 0 (no phase locking) and 1 (perfect phase locking across time). PLV was calculated for each subject with a 2-min artifact-free segment epoched into 4-s segments and averaged across segments (Stam et al. 2009). The PLV matrices for the beta band were averaged across the five beta bands. Thus each subject had four adjacency matrices (1 per frequency band) of 5,000 × 5,000 nodes representing connectivity between all dipoles.

Graph theory analysis. Graph analysis is a type of complex network analysis that helps describe network topologies in terms of features that can be related to neural function and organization (Rubinov and Sporns 2010). Network features can be grouped into two large groups, features describing functional segregation and global integration. Functional segregation quantifies the presence of local groups showing specialized functions relative to the rest of the network, while global integration describes the efficiency with which the network integrates the information flow from all of these functionally segregated clusters across the network.

For graph analysis, we used the PLV matrices as undirected weighted adjacency matrix (Bullmore and Sporns 2009) where the weight of the connection between two nodes in the network is defined as the PLV between those nodes. The inverse of the PLV represented the length of the path needed to travel between nodes where more strongly connected nodes would have shorter path lengths.

We calculated two graph theory metrics: the clustering coefficient (C_w) (van Dellen et al. 2012) and global efficiency (Rubinov and Sporns 2010). C_w describes the functional segregation of local clusters by measuring the likelihood that nodes connected to a given node are also connected to each other. Global and local efficiency are measures of global integration. The global efficiency represents the average of the efficiency of communication between all pair combinations across a network. Mathematically, it represents the average inverse shortest path length (Latora and Marchiori 2001). Local efficiency describes how efficient the communication between the neighbors of a node becomes if that node is removed. Neither metric was normalized to surrogate random networks. While this correction is needed for smaller networks (<100 nodes), the size of the network used in this analysis (5,000 nodes) is well above the limit of 200 nodes at which graph metrics are less susceptible to variations in network size and density (van Wijk et al. 2010).

Statistical analysis. The global PLV differences between the two groups were calculated by averaging the PLVs for the entire adjacency matrix for each subject. Differences in the medians of two groups were assessed with the nonparametric Wilcoxon signed-rank test. The statistical significance of PLV differences between the two groups at the source dipole level was examined with nonparametric cluster-based permutation testing (Maris and Oostenveld 2007). This method is insensitive to outlier effects considering the small number of subjects. All subjects were pooled, and in each permutation subjects were randomly assigned to one of the two groups. A t-test was then performed between the two groups. The resulting t-statistic image was threshholded at voxel P value of 0.01 corresponding to a t-statistic of 2.326. The significant t-statistic voxels were then clustered based on the x, y, and z locations of the source dipole. We performed 200 random permutations and then generated a null distribution of cluster t-statistics sums. Clusters in the actual data were assigned a P value based on the percentile of the permuted distribution to which they correspond. To correct for multiple comparisons for the multiple frequency bands, only clusters with a P value < 0.0125 were considered significant (Bonferroni correction for 4 frequency bands).

Comparisons of the different graph analysis metrics were performed with the nonparametric Wilcoxon signed-rank test between the median values of the dipoles falling in a ROI. All statistical calculations were performed with MATLAB.

RESULTS

Phase synchrony. The global mean PLVs were similar but showed a trend toward a decrease in the mTBI group for the delta (z value −1.37, P value 0.17), theta (z value −0.05, P value 0.95), alpha (z value −1.35, P value 0.15), and beta (z value −1.311, P value 0.189) frequency bands. For every group average connectivity matrix, the PLVs above the 90th

Fig. 2. Group average connectivity across groups. Phase locking values were averaged across subjects and across ROIs. Only the values above the 90th quantile of the averaged data are displayed for simplicity. Each line represents a connection between the 2 ROIs with the color signifying the strength of the connection in terms of PLV. *A*, *C*, and *E* represent the group-average PLV for the control group in the delta, alpha, and beta frequencies, respectively. *B*, *D*, and *F* represent the group-average PLV for the control group in the delta, alpha, and beta frequencies, respectively. Labels represent the anatomically parcellated regions based on FreeSurfer autosegmentation. Brain regions are grouped anatomically by lobe, as indicated by color coding.

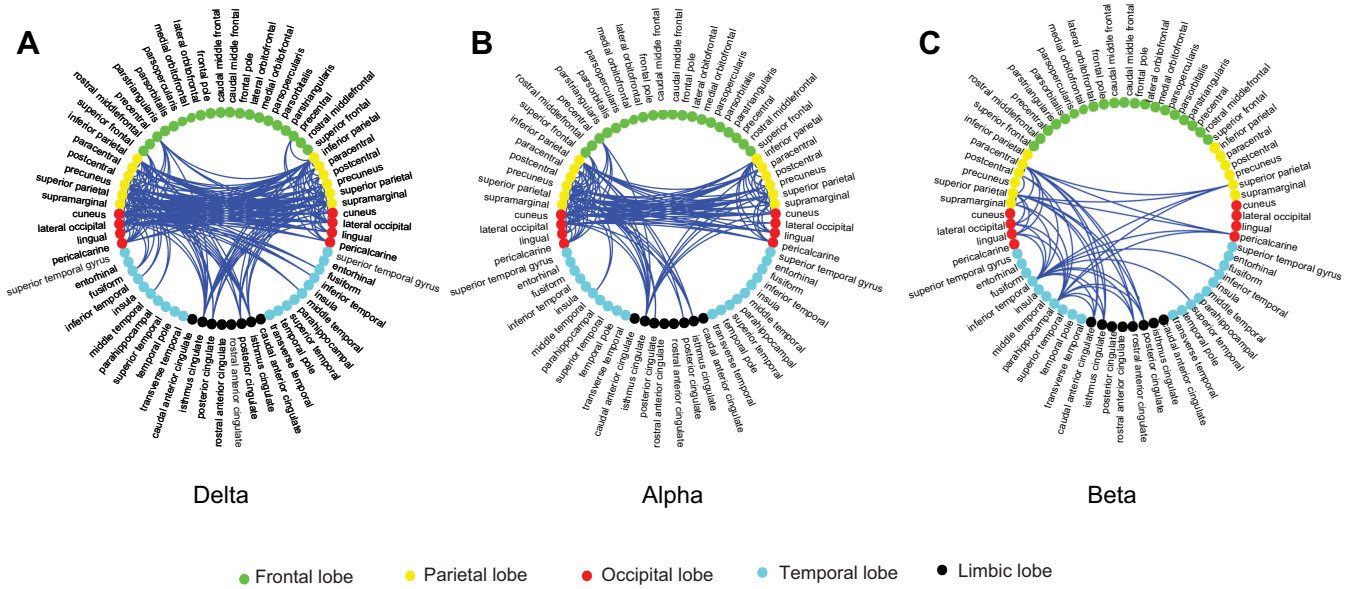

Fig. 3. Connectivity plots representing mTBI-related reductions. *A*, *B*, and *C* represent the PLV reduction in the delta, alpha, and beta frequencies, respectively. Each line represents a connection showing a statistically significant reduction in PLV in the mTBI group, compared with control subjects, between the labeled regions. Labels represent the anatomically parcellated regions in which dipoles with statistically significant clusters ($P < 0.0125$) were located. Brain regions are grouped anatomically by lobe, as indicated by color coding.

quantile were retained and are displayed in Fig. 2. To identify the regions contributing to the reduction in phase locking we used permutation testing to identify spatial clustering, based on the *x*, *y*, and *z* locations of the source dipoles. Regions of spatially connected dipoles forming clusters of nodes with similarly patterned connections were identified in all frequency bands on the *t*-statistic map of difference in PLV values between the mTBI and control groups (cluster *P* value of 0.05). To control for the number of frequency bands studied, we rejected any clusters above a corrected *P* value of 0.0125 (Bonferroni correction). The theta frequency did not have any clusters below the corrected *P* value of 0.0125. Multiple clusters were found in the delta, alpha, and beta bands with a *P* value < 0.0125.

PLV was reduced in mTBI most frequently for clusters in the delta frequency band. The connections showing this reduction in delta phase locking involved both intralobar and interlobar connections. Although interhemispheric connections showed reduced connectivity predominantly in the delta band, alpha and beta frequency phase locking were also reduced. Anatomically, the largest number of connections showing a reduction in phase locking were found within the parietal and occipital lobes in each frequency band. Reduced beta phase locking in the mTBI group was most prominent in the temporal lobe. Of note, these PLV reductions in the mTBI group occurred in major hubs of the DMN, including the posterior cingulate cortex (PCC), inferior parietal lobule, and precuneus gyrus. The network topology for delta, alpha, and beta frequency bands is detailed in Fig. 3, *A*, *B*, and *C*, respectively.

Graph theory. Global integration measures used to evaluate the efficiency with which the network integrates information flow from segregated clusters did not reveal a statistically significant difference in medians between groups ($P > 0.05$, Wilcoxon rank sum test). Functional segregation analysis to quantify the presence of local groups, however, demonstrated that local efficiency was reduced in the concussion group compared with the control group in all frequency bands for the regions detailed in Table 2 ($P < 0.05$ uncorrected). No statistically significant clustering coefficient changes were found between the two groups.

DISCUSSION

In this study we used PLV and graph theory in a data-driven manner to investigate mTBI-related changes in whole brain functional connectivity in patients showing persistent postconcussive symptoms. To our knowledge, this is the first study to demonstrate that MEG can detect mTBI network changes at the source level. Our results show that the reduction in PLV

Table 2. *Cortical regions with reduced regional efficiency subdivided by frequency band*

	δ (1–4 Hz)	θ (4–8 Hz)	α (8–12 Hz)	β (13–30 Hz)
Regions showing reduced regional efficiency	Superior parietal lobule Cuneus Inferior parietal Lateral occipital Supramarginal	Superior parietal lobule	Superior parietal lobule Cuneus Inferior parietal Lateral occipital Precuneus	Superior parietal lobule

Cortical regions where source dipoles showed a reduction in local efficiency in the mTBI group compared with control subjects at an uncorrected level are shown. Each column represents the frequency band at which functional connectivity was evaluated. The labels represent the anatomical regions parcellated with FreeSurfer that had dipoles with reduced regional efficiency.

following mTBI is not a global effect but involves a specific network of cortical regions. The size and extent of this network vary across the different frequencies of neuronal oscillations. The network involved spanned the temporal, parietal, occipital, and cingulate cortical regions. Of note, the inferior parietal and precuneus cortical regions showed the largest number of connectivity changes. Our findings also highlight the loss of both regional intralobar connectivity and interhemispheric connectivity.

Our findings are in line with current research describing a network topology and band-specific changes in mTBI. Changes in alpha band connectivity have been demonstrated across TBI patients of varying severity (Tarapore et al. 2013). Alpha slowing and shift of the alpha peak to a lower frequency has been observed after mTBI (Dunkley et al. 2015), and a classification tool based on alpha connectivity that identifies mTBI with high predictive accuracy has been reported (Dimitriadis et al. 2015). For the delta frequency, previous work has demonstrated the generation of slow waves following TBI that are hypothesized to stem from white matter deafferentation (Huang et al. 2014; Lewine et al. 1999), as suggested by animal studies (Ball et al. 1977; Gloor et al. 1977). A postulated mechanism for the loss of white matter integrity following mTBI is diffuse axonal injury. One hypothesis for the emergence of subsequent cognitive impairment is that deafferentation leads to the generation of areas with asynchronous delta activity and functional disconnection. The overlap in network topography between the alpha and delta networks suggests that they might share a common causal mechanism. Supporting this hypothesis, the extent of white matter damage observed with tractography after mTBI was shown to correlate with the degree of reduction in functional connectivity (Sharp et al. 2011).

In terms of the observed network topology, the structure of the alpha band network showing reduction in mTBI matches that of the dominant network described by Hillebrand and colleagues in the healthy state for the alpha band (Hillebrand et al. 2012). The network consisted of the visual cortex and the parietal and temporal lobes in addition to the PCC. These regions represent major hubs in the DMN (Raichle et al. 2001). It has been proposed that while an individual is at rest the DMN exhibits highly coordinated activity that is subsequently deactivated during task performance (Raichle et al. 2001). The core nodes of the DMN are thought to include the PCC, the precuneus, and the medial prefrontal cortex. Functionally, the DMN has been linked to internally driven attention and the performance of automatic behavior (Mason et al. 2007). Both the activity and functional connectivity within the DMN were linked to performance in higher cognitive functions such as memory and attention (Buckner et al. 2008; Hampson et al. 2006; Leech et al. 2011), deficits that are the most common reported consequences of mTBI (van der Naalt et al. 1999; Smith-Seemiller et al. 2003). fMRI-based studies have documented DMN dysfunction after mTBI (Mayer et al. 2011; Nathan et al. 2015; Palacios et al. 2013; Sharp et al. 2011; Sours et al. 2013; Stevens et al. 2012; Zhou et al. 2012) and in several disease states such as ADHD, Alzheimer's disease, and schizophrenia (Koch et al. 2012; Uddin et al. 2008; Whitfield-Gabrieli et al. 2009).

Given the association between the DMN and cognitive functions such as working memory and attention (Buckner et al. 2008; Hampson et al. 2006; Leech et al. 2011), our findings suggest that this disconnection in the DMN might play a role in the cognitive deficits seen in postconcussion patients and might be a potential prognostic factor. The loss of interhemispheric connections may be explained by damage to fibers in the corpus callosum, given that there is tractography evidence for matter damage to these fibers after TBI (Fagerholm et al. 2015).

One major limitation of this study is the relatively small number of subjects recruited and the relative heterogeneity in this subject cohort with regard to age and time since injury. Furthermore, the large number of observations between every pair combination of dipole locations and frequency band would require very large effect sizes to be considered significant to account for the large number of multiple comparisons. We sought to address all of these issues through permutation testing with cluster-based correction for multiple comparisons based on spatial clustering. If any of the observed group differences are driven by only a handful of the subjects, shuffling the subjects across the two groups would distribute this effect into the surrogate distribution and thus control their significance level. Such cluster-based correction is a validated method to correct for multiple comparisons that is sensitive to smaller effect sizes (Maris and Oostenveld 2007).

Graph theory analysis helps describe the functional characteristics of multidimensional, complex connectivity matrices. We applied graph theory analysis to localize the network nodes affected by mTBI based on changes in their functional characteristics. The results are in line with the phase locking connectivity changes observed, where global efficiency is relatively preserved but specific hubs become partially disconnected. Dimitriadis and colleagues reached similar conclusions, where they found no differences in global efficiency compared with healthy subjects and a reduction in local efficiency across all frequency bands (except the theta band at an uncorrected *P*-value level) (Dimitriadis et al. 2015). These results suggest that while the whole brain network has a similar degree of efficiency in connections in the mTBI group compared with healthy control subjects, the pathological changes are more localized to certain critical regions. We cannot rule out that the data also could reflect statistical power limitations in detecting subtle changes in the number of subjects in our cohort. Alternatively, the data may reflect plasticity changes that compensate for the reduced efficiency in parts of the network. It is also important to note that changes in global efficiency might become more evident during nonresting behavior, when the affected nodes are engaged in active cognitive tasks.

Despite the short duration of the recordings used compared with other studies (Dimitriadis et al. 2015), we observed robust connectivity relationships, similar to previous descriptions of a stable network topology being achieved from smaller time segments (Chu et al. 2012; van Dellen et al. 2014). Even shorter time segments (~60 s) have been reported to be adequate for capturing group connectivity differences in Alzheimer's disease (Stam et al. 2009) and Parkinson's disease (Olde Dubbelink et al. 2014). Our data suggest that one strength of a MEG-based evaluation of subjects with mTBI is that a short duration (2–4 min) of resting-state recordings can provide useful information regarding the status of functional connectivity.

Limitations. While the results show a robust change in the major hubs of the DMN, we are not able to link these findings to any specific cognitive changes within this cohort of subjects, as neuropsychological testing scores were not available for all subjects. While resting-state analysis was used because of the ease of administration in mTBI subjects, inferring the functional outcome of these changes requires functional imaging studies during task conditions that engage these areas of interest and correlating the task performance with the functional changes observed (Kida et al. 2016). We hope to address this issue in further studies.

Of note, PLV is sensitive to false positives due to zero-phase lag that can be introduces by field spread caused by imperfections in the inverse solution. Multiple methods have been developed to circumvent this issue, from using phase synchrony measures less sensitive to zero-phase lag like the phase lag index (Stam et al. 2007) to using regression models prior to calculating connectivity (Brookes et al. 2012) or simply subtracting a randomly generated phase locking matrix by projecting noise using the same inverse solution (Ghuman et al. 2011). As discussed in Ghuman et al. (2011), this issue is addressed by the fact that the results shown are *t*-statistic differences; thus any signal spread introduced through the inverse solution would be in all the subjects and should not be seen in the contrast between groups.

Conclusions. MEG can be used to detect and quantify widespread network disruption resulting from mTBI, even months after the initial insult. These data suggest that regions involved in the DMN may contribute to the persistence of cognitive symptoms experienced by many patients after mTBI.

DISCLOSURES

No conflicts of interest, financial or otherwise, are declared by the author(s).

AUTHOR CONTRIBUTIONS

A.A., T.A.W., D.K., and A.S.G. analyzed data; A.A., T.A.W., D.K., S.P., S.A.W., A.S.G., and R.M.R. interpreted results of experiments; A.A., T.A.W., and R.M.R. prepared figures; A.A., T.A.W., A.S.G., R.M.R., and A.N. drafted manuscript; A.A., T.A.W., A.S.G., R.M.R., and A.N. edited and revised manuscript; A.A., A.S.G., D.O.O., R.M.R., and A.N. approved final version of manuscript; S.P., S.A.W., D.N.K., D.O.O., and A.N. conception and design of research; S.A.W., D.N.K., D.O.O., and A.N. performed experiments.

REFERENCES

Centers for Disease Control and Prevention. *Report to Congress on Mild Traumatic Brain Injury in the United States: Steps to Prevent a Serious Public Health Problem*. Atlanta, GA: National Center for Injury Prevention and Control, 2003.

Centers for Disease Control and Prevention. *Report to Congress on Traumatic Brain Injury in the United States: Epidemiology and Rehabilitation*. Atlanta, GA: National Center for Injury Prevention and Control; Division of Unintentional Injury Prevention, 2014. http://www.cdc.gov/traumaticbraininjury/pdf/TBI_Report_to_Congress_Epi_and_Rehab-a.pdf.

Baillet S, Mosher JC, Leahy RM. Electromagnetic brain mapping. *IEEE Signal Process Mag* 18: 14–30, 2001.

Ball GJ, Gloor P, Schaul N. The cortical electromicrophysiology of pathological delta waves in the electroencephalogram of cats. *Electroencephalogr Clin Neurophysiol* 43: 346–361, 1977.

Van Boven RW, Harrington GS, Hackney DB, Ebel A, Gauger G, Bremner JD, D'Esposito M, Detre JA, Haacke EM, Jack CR, Jagust WJ, Le Bihan D, Mathis CA, Mueller S, Mukherjee P, Schuff N, Chen A, Weiner MW. Advances in neuroimaging of traumatic brain injury and posttraumatic stress disorder. *J Rehabil Res Dev* 46: 717–757, 2009.

Brookes MJ, Woolrich MW, Barnes GR. Measuring functional connectivity in MEG: a multivariate approach insensitive to linear source leakage. *Neuroimage* 63: 910–920, 2012.

Buckner RL, Andrews-Hanna JR, Schacter DL. The brain's default network: anatomy, function, and relevance to disease. *Ann NY Acad Sci* 1124: 1–38, 2008.

Bullmore E, Sporns O. Complex brain networks: graph theoretical analysis of structural and functional systems. *Nat Rev Neurosci* 10: 186–198, 2009.

Castellanos NP, Leyva I, Buldú JM, Bajo R, Paúl N, Cuesta P, Ordóñez VE, Pascua CL, Boccaletti S, Maestú F, del-Pozo F. Principles of recovery from traumatic brain injury: reorganization of functional networks. *Neuroimage* 55: 1189–1199, 2011.

Chu CJ, Kramer MA, Pathmanathan J, Bianchi MT, Westover MB, Wizon L, Cash SS. Emergence of stable functional networks in long-term human electroencephalography. *J Neurosci* 32: 2703–2713, 2012.

Cicerone KD, Kalmar K. Persistent postconcussion syndrome: the structure of subjective complaints after mild traumatic brain injury. *J Head Trauma Rehabil* 10: 1–17, 1995.

van Dellen E, Douw L, Hillebrand A, Ris-Hilgersom IH, Schoonheim MM, Baayen JC, De Witt Hamer PC, Velis DN, Klein M, Heimans JJ, Stam CJ, Reijneveld JC. MEG network differences between low- and high-grade glioma related to epilepsy and cognition. *PLoS One* 7: e50122, 2012.

van Dellen E, van der Kooi AW, Numan T, Koek HL, Klijn FA, Buijsrogge MP, Stam CJ, Slooter AJ. Decreased functional connectivity and disturbed directionality of information flow in the electroencephalography of intensive care unit patients with delirium after cardiac surgery. *Anesthesiology* 121: 328–335, 2014.

Delorme A, Makeig S. EEGLAB: an open source toolbox for analysis of single-trial EEG dynamics including independent component analysis. *J Neurosci Methods* 134: 9–21, 2004.

Destrieux C, Fischl B, Dale A, Halgren E. Automatic parcellation of human cortical gyri and sulci using standard anatomical nomenclature. *Neuroimage* 53: 1–15, 2010.

Dimitriadis SI, Zouridakis G, Rezaie R, Babajani-Feremi A, Papanicolaou AC. Functional connectivity changes detected with magnetoencephalography after mild traumatic brain injury. *Neuroimage Clin* 9: 519–531, 2015.

Dunkley BT, Da Costa L, Bethune A, Jetly R, Pang EW, Taylor MJ, Doesburg SM. Low-frequency connectivity is associated with mild traumatic brain injury. *Neuroimage Clin* 7: 611–621, 2015.

Fagerholm ED, Hellyer PJ, Scott G, Leech R, Sharp DJ. Disconnection of network hubs and cognitive impairment after traumatic brain injury. *Brain* 138: 1696–1709, 2015.

Fischl B, Sereno MI, Tootell RB, Dale AM. High-resolution intersubject averaging and a coordinate system for the cortical surface. *Hum Brain Mapp* 8: 272–284, 1999.

Fries P. Rhythms for cognition: communication through coherence. *Neuron* 88: 220–235, 2015.

Ghuman AS, McDaniel JR, Martin A. A wavelet-based method for measuring the oscillatory dynamics of resting-state functional connectivity in MEG. *Neuroimage* 56: 69–77, 2011.

Gloor P, Ball G, Schaul N. Brain lesions that produce delta waves in the EEG. *Neurology* 27: 326–333, 1977.

Hampson M, Driesen NR, Skudlarski P, Gore JC, Constable RT. Brain connectivity related to working memory performance. *J Neurosci* 26: 13338–13343, 2006.

Hillebrand A, Barnes GR, Bosboom JL, Berendse HW, Stam CJ. Frequency-dependent functional connectivity within resting-state networks: an atlas-based MEG beamformer solution. *Neuroimage* 59: 3909–3921, 2012.

Huang MX, Mosher JC, Leahy RM. A sensor-weighted overlapping-sphere head model and exhaustive head model comparison for MEG. *Phys Med Biol* 44: 423–440, 1999.

Huang MX, Nichols S, Baker DG, Robb A, Angeles A, Yurgil KA, Drake A, Levy M, Song T, McLay R, Theilmann RJ, Diwakar M, Risbrough VB, Ji Z, Huang CW, Chang DG, Harrington DL, Muzzatti L, Canive JM, Edgar JC, Chen YH, Lee RR. Single-subject-based whole-brain MEG slow-wave imaging approach for detecting abnormality in patients with mild traumatic brain injury. *Neuroimage Clin* 5: 109–119, 2014.

Kida T, Tanaka E, Kakigi R. Multi-dimensional dynamics of human electromagnetic brain activity. *Front Hum Neurosci* 9: 713, 2016.

Koch W, Teipel S, Mueller S, Benninghoff J, Wagner M, Bokde AL, Hampel H, Coates U, Reiser M, Meindl T. Diagnostic power of default mode network resting state fMRI in the detection of Alzheimer's disease. *Neurobiol Aging* 33: 466–478, 2012.

Lachaux JP, Rodriguez E, Martinerie J, Varela FJ. Measuring phase synchrony in brain signals. *Hum Brain Mapp* 8: 194–208, 1999.

Latora V, Marchiori M. Efficient behavior of small-world networks. *Phys Rev Lett* 87: 198701, 2001.

Leech R, Kamourieh S, Beckmann CF, Sharp DJ. Fractionating the default mode network: distinct contributions of the ventral and dorsal posterior cingulate cortex to cognitive control. *J Neurosci* 31: 3217–3224, 2011.

Lewine JD, Davis JT, Sloan JH, Kodituwakku PW, Orrison WW. Neuromagnetic assessment of pathophysiologic brain activity induced by minor head trauma. *AJNR Am J Neuroradiol* 20: 857–866, 1999.

Liu Z, Fukunaga M, de Zwart JA, Duyn JH. Large-scale spontaneous fluctuations and correlations in brain electrical activity observed with magnetoencephalography. *Neuroimage* 51: 102–111, 2010.

Maris E, Oostenveld R. Nonparametric statistical testing of EEG- and MEG-data. *J Neurosci Methods* 164: 177–190, 2007.

Mason MF, Norton MI, Van Horn JD, Wegner DM, Grafton ST, Macrae CN. Wandering minds: the default network and stimulus-independent thought. *Science* 315: 393–395, 2007.

Mayer AR, Mannell MV, Ling J, Gasparovic C, Yeo RA. Functional connectivity in mild traumatic brain injury. *Hum Brain Mapp* 32: 1825–1835, 2011.

van der Naalt J, van Zomeren AH, Sluiter WJ, Minderhoud JM. One year outcome in mild to moderate head injury: the predictive value of acute injury characteristics related to complaints and return to work. *J Neurol Neurosurg Psychiatry* 66: 207–213, 1999.

Nathan DE, Oakes TR, Yeh PH, French LM, Harper JF, Liu W, Wolfowitz RD, Wang BQ, Graner JL, Riedy G. Exploring variations in functional connectivity of the resting state default mode network in mild traumatic brain injury. *Brain Connect* 5: 102–114, 2015.

Olde Dubbelink KT, Hillebrand A, Stoffers D, Deijen JB, Twisk JW, Stam CJ, Berendse HW. Disrupted brain network topology in Parkinson's disease: a longitudinal magnetoencephalography study. *Brain* 137: 197–207, 2014.

Palacios EM, Sala-Llonch R, Junque C, Roig T, Tormos JM, Bargallo N, Vendrell P. Resting-state functional magnetic resonance imaging activity and connectivity and cognitive outcome in traumatic brain injury. *JAMA Neurol* 70: 845–851, 2013.

Raichle ME, MacLeod AM, Snyder AZ, Powers WJ, Gusnard AD, Shulman GL. A default mode of brain function. *Proc Natl Acad Sci USA* 98: 676–682, 2001.

Rubinov M, Sporns O. Complex network measures of brain connectivity: uses and interpretations. *Neuroimage* 52: 1059–1069, 2010.

Sharp DJ, Beckmann CF, Greenwood R, Kinnunen KM, Bonnelle V, De Boissezon X, Powell JH, Counsell SJ, Patel MC, Leech R. Default mode network functional and structural connectivity after traumatic brain injury. *Brain* 134: 2233–2247, 2011.

Sharp DJ, Scott G, Leech R. Network dysfunction after traumatic brain injury. *Nat Rev Neurol* 10: 156–166, 2014.

Smith-Seemiller L, Fow NR, Kant R, Franzen MD. Presence of post-concussion syndrome symptoms in patients with chronic pain vs. mild traumatic brain injury. *Brain Inj* 17: 199–206, 2003.

Sours C, Zhuo J, Janowich J, Aarabi B, Shanmuganathan K, Gullapalli RP. Default mode network interference in mild traumatic brain injury—a pilot resting state study. *Brain Res* 1537: 201–215, 2013.

Stam CJ, de Haan W, Daffertshofer A, Jones BF, Manshanden I, van Cappellen van Walsum AM, Montez T, Verbunt JP, de Munck JC, van Dijk BW, Berendse HW, Scheltens P. Graph theoretical analysis of magnetoencephalographic functional connectivity in Alzheimer's disease. *Brain* 132: 213–224, 2009.

Stam CJ, Nolte G, Daffertshofer A. Phase lag index: assessment of functional connectivity from multi channel EEG and MEG with diminished bias from common sources. *Hum Brain Mapp* 28: 1178–1193, 2007.

Stevens MC, Lovejoy D, Kim J, Oakes H, Kureshi I, Witt ST. Multiple resting state network functional connectivity abnormalities in mild traumatic brain injury. *Brain Imaging Behav* 6: 293–318, 2012.

Tadel F, Baillet S, Mosher JC, Pantazis D, Leahy RM. Brainstorm: a user-friendly application for MEG/EEG analysis. *Comput Intell Neurosci* 2011: 879716, 2011.

Tarapore PE, Findlay AM, Lahue SC, Lee H, Honma SM, Mizuiri D, Luks TL, Manley GT, Nagarajan SS, Mukherjee P. Resting state magnetoencephalography functional connectivity in traumatic brain injury. *J Neurosurg* 118: 1306–1316, 2013.

Uddin LQ, Kelly AM, Biswal BB, Margulies DS, Shehzad Z, Shaw D, Ghaffari M, Rotrosen J, Adler LA, Castellanos FX, Milham MP. Network homogeneity reveals decreased integrity of default-mode network in ADHD. *J Neurosci Methods* 169: 249–254, 2008.

Vanderploeg RD, Curtiss G, Belanger HG. Long-term neuropsychological outcomes following mild traumatic brain injury. *J Int Neuropsychol Soc* 11: 228–236, 2005.

Whitfield-Gabrieli S, Thermenos HW, Milanovic S, Tsuang MT, Faraone SV, McCarley RW, Shenton ME, Green AI, Nieto-Castanon A, LaViolette P, Wojcik J, Gabrieli JD, Seidman LJ. Hyperactivity and hyperconnectivity of the default network in schizophrenia and in first-degree relatives of persons with schizophrenia. *Proc Natl Acad Sci USA* 106: 1279–1284, 2009.

van Wijk BC, Stam CJ, Daffertshofer A. Comparing brain networks of different size and connectivity density using graph theory. *PLoS One* 5: e13701, 2010.

Zhou Y, Milham MP, Lui YW, Miles L, Reaume J, Sodickson DK, Grossman RI, Ge Y. Default-mode network disruption in mild traumatic brain injury. *Radiology* 265: 882–992, 2012.